

Enhancing Synthetic Oversampling for Imbalanced Datasets Using Proxima-Orion Neighbors and q-Gaussian Weighting Technique

Pankaj Yadav , Vivek Vijay and Gulshan Sihag

Abstract—In this article, we propose a novel oversampling algorithm to increase the number of instances of minority class in an imbalanced dataset. We select two instances, Proxima and Orion, from the set of all minority class instances, based on a combination of relative distance weights and density estimation of majority class instances. Furthermore, the q-Gaussian distribution is used as a weighting mechanism to produce new synthetic instances to improve the representation and diversity. We conduct a comprehensive experiment on 42 datasets extracted from KEEL software and eight datasets from the UCI ML repository to evaluate the usefulness of the proposed (PO-QG) algorithm. Wilcoxon signed-rank test is used to compare the proposed algorithm with five other existing algorithms. The test results show that the proposed technique improves the overall classification performance. We also demonstrate the PO-QG algorithm to a dataset of Indian patients with sarcopenia.

Index Terms—oversampling, data generation, class imbalance, proxima-orion neighbors, q-gaussian distribution.

I. INTRODUCTION

Traditional machine learning classification methods assume balanced data distributions and aim to maximize overall accuracy. In case of an imbalanced dataset, the uneven class distribution makes the model biased toward the majority class, resulting in poor performance of the underlying model [1]. Although this issue of imbalance nature of the data is crucial in every field, but in the field of healthcare and finance, it becomes more critical due to the importance of the minority class. For example, rare diseases, due to their low occurrence, having an underrepresented class [2] may lead to misdiagnosis, resulting in life-threatening cases while predicting the disease. Similarly, in the field of finance, this misrepresentation of the minority class can have several impacts on fraud detection [3]. In imbalanced classification situations, the binary technique often serves as a standard case. Multi-class datasets are modified into binary classes using standard techniques like one vs all (OVA) or one vs one (OVO). These modifications sometimes increase the imbalance, especially when the minority class is further split, resulting in more significant challenges in effectively modeling the data. Therefore, correct identification of the minority class is essential due to its significant cost of misclassification in real-world situations [4].

Pankaj Yadav is a Research Scholar in the Department of Mathematics, Indian Institute of Technology Jodhpur, India. (email: yadav.58@iitj.ac.in)

Vivek Vijay is with the Department of Mathematics, Indian Institute of Technology Jodhpur, India. (email: vivek@iitj.ac.in)

UPHF, CNRS, UMR 8201 - LAMIH, Valenciennes, F-59313, France.(email: sihag.1@alumni.iitj.ac.in)

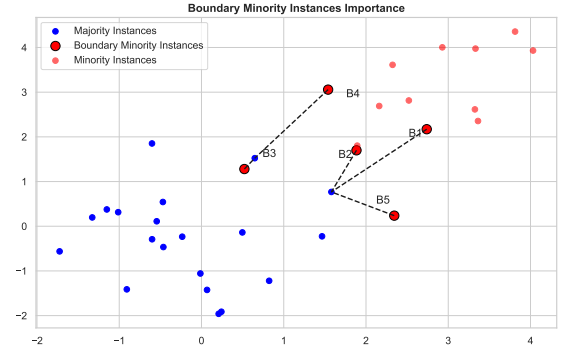


Fig. 1: Boundary Minority Instances and Their Proximity to Majority Instances

In machine learning models, a classifier applied directly without balancing does not perform well. Several strategies have been developed to address the issue of imbalance nature of the data. These strategies are categorized into data-level, algorithmic-level and cost-sensitive approaches. Data-level methods [5], [6] focus on modifying the training data to fix the class imbalance. These methods either generate the samples in the minority class or eliminate the instances in the majority class [7]. These approaches are favored as these methods do not depend on the underlying classifiers [8], [9], [10] [11]. This makes them widely applicable and is the central theme of this research also. Some popularly used methods include the synthetic minority oversampling technique (SMOTE) [12]. Although SMOTE is an effective method, it is an unstrategic oversampling technique. Improved variants of SMOTE, such as SMOTE-Tomek Link [13], SMOTE-ENN [14], [15] and Borderline Smote [16], provide some improvement over the original algorithm, while facing significant drawbacks. All these variants of SMOTE struggle to preserve the original data distribution and do not effectively capture the complex distribution of the minority data. Second, both the distribution and distance of the classes play a crucial role in determining the quality of the generated samples. Boundary minority instances, located near the decision boundary between the majority and minority classes, are particularly sensitive to misclassification.

In Figure 1, "B3" may be situated at the boundary of a cluster of majority instances. This position increases its vulnerability to misclassification as a majority instance.

The closeness of the boundary minority instances to the majority class can affect the decision boundary. Inappropriate classification of these classes by the model may result in an inadequately defined decision boundary. This leads to a decrease in the model's accuracy in predicting minority class classes. Therefore, it is crucial to strategically place the synthetic instances near the boundary to ensure that the decision boundary is accurately represented.

Congjun Rao et al. proposed a technique known as the adaptive double weights and Gaussian kernel function oversampling (ADWGKFO) for handling the imbalance in cardiovascular disease (CVD) datasets [17]. The approach clusters minority samples, identifies boundary samples, and calculates the number of synthesized samples using double weights of boundary points and majority distribution. It further improves new samples using the Gaussian kernel function to filter. However, similar to SMOTE variants, ADWGKFO may still face challenges in not being able to correctly capture the full complexity of minority class distribution when dealing with highly irregular and overlapping classes. Yongxu Liu et al. Proposed a noise-robust oversampling algorithm designed for mixed-type and multi-class imbalance data. They tackle the overlapping issues by eliminating noise with clusters and using adaptive embedding to generate safer samples [18]. The approach expands the class boundary via a secure border mechanism suitable for complex datasets. However, despite its algorithmic strength against noise, it may encounter difficulties ensuring that the generated samples appropriately represent distribution of minority classes in datasets with poorly defined class boundaries. Yuxi Xie, Min Qiu, Haibo Zhang, et al. introduced the Gaussian distribution-based oversampling approach. The new minority instances are generated following the Gaussian distribution model [19]. The method shows improved performance on various datasets. However, GDO's dependency on Gaussian distribution may limit its ability to learn more complex and nonlinear data structures. It may also lead to potential inaccuracies in generating representative minority samples. Michał Koziarski et al. proposed the Synthetic Minority Undersampling Technique with its combination with SMOTE (SMUTE) and Combined Synthetic Oversampling and Undersampling Technique (CSMOUTE) [20]. SMUTE uses interpolation to undersample the majority of instances, while CSMOUTE integrates this method with SMOTE oversampling. Experiments revealed that these methods, when paired with complex classifiers like MLP and SVM significantly manage datasets having several outliers. These methods may still be inadequate because of their interpolation-based techniques, when dealing with overlapping and irregular minority classes.

Ensemble-based techniques: These machine learning methodologies combine the predictions of multiple models to improve the overall performance [21] and help reduce model bias and variance by integrating different classifiers. Popular ensemble methods like bagging, boosting, and random forest [?], [22] have been adapted to address the class imbalance and ensure the minority classes receive adequate

representation in the final model decisions. R. Nithya et al. propose an algorithm that uses ensemble learning with the Support Vector Machine-Synthetic Minority Oversampling Technique (SVM-SMOTE) to address imbalances in cerebrovascular disease datasets [23]. The method combines preprocessing, SVM-SMOTE, and various ensemble methods to improve classification accuracy. Liang et al. Propose a Bagging Ensemble Learning Framework, namely Anomaly Scoring Based Ensemble Learning, to address the high imbalance rate shown in binary classification tasks [24]. He et al. propose the Multi-Objective Selective Ensemble (MMSE) Framework that addresses trade-offs in multi-class imbalance by using selective ensemble learning and multiple undersampling rates [25]. Additionally, Nur Hanisah Abdul Malek et al. Investigate the impact of class imbalance on water quality data using a range of classifiers and sampling approaches [26]. They found that while gradient boosting and random forest performed best without resampling, for most matrices, balanced accuracy and sensitivity improved with random undersampling and complete resampling, respectively.

Cost-sensitive learning: These techniques directly use the cost of misclassification in the training process [27]. Other traditional methods focus only on balancing the dataset, while cost-sensitive approaches adjust the learning algorithm to account for the higher costs associated with misclassifying the minority class instances. This can be achieved by allocating the different weights to classes and misclassification errors [28]. This guides the model to pay more attention to the minority class. In multi-view imbalance learning, Zhaojie Hou et al. introduced a multi-view instance-level cost-sensitive SVM with QTSE loss (MVQS) to handle datasets with multi-view representations, imbalanced classes, and noisy instances [29]. This approach uses consensus regularization and a combination weight strategy to fully exploit multi-view information. In order to optimize data distribution, Kaixiang Yang et al. introduce the Imbalanced Large Margin Nearest Neighbor (ILMNN) approach. ILMNN uses metric learning to establish a latent feature space that refines the sample distribution [30]. The refinement is done by pulling intra-class samples closer and distancing intra-class samples. This improves the performance of oversampling techniques. Similarly, Xinqi Li et al. Proposed DDSC-SMOTE, an oversampling algorithm that addresses SMOTE's limitation by using data distribution and spectral clustering-based strategies [31]. DDSC-SMOTE uses adaptive allocation of synthetic samples, seed sample selection, and improvements to the SMOTE synthesis formula. These improvements significantly outperform existing methods in terms of performance on real datasets.

In order to address these challenges, we propose PO-QG(Proxima-Orion & Q-Gaussian) oversampling, a novel algorithm designed to improve synthetic minority instance generation through two-step process:

- PO-QG identifies two minority neighbors (Proxima and Orion) based on relative distance weighting and majority class density estimation. This ensure the

selected neighbors are representative and informative with generation of synthetic samples that correctly reflect the complexity of the minority class.

- Using a q-Gaussian distribution, PO-QG assigns normalized weights derived from the distances between the minority instance and its neighbor. These weights generate diverse, representative synthetic samples which improves classification performance on imbalanced datasets.

By producing high quality synthetic instances, PO-QG addresses limitations in existing method that leads to improved classification outcomes across a broad range of applications. The paper is structured as follows: Section II outlines the details of our proposed methodology. Section III and IV presents case study results and analyzes the experimental outcomes respectively. Section V concludes the paper and outlines future work.

II. PROXIMA-ORION & Q-GAUSSIAN OVERSAMPLING

The Proxima-Orion & Q-Gaussian(PO-QG) Oversampling aims to improve the performance of the minority class by synthesizing new instances. It utilizes a dual-phase methodology as shown in Fig 2. In the first step, Proxima and Orion neighbors are selected based on relative distance and density. Second, synthetic instances are generated using q-Gaussian weights.

The initial phase of the method randomly selects the anchor minority instances. Subsequently, the algorithm identifies the nearest minority neighbors using the k-nearest neighbors [32] (k-NN) approach. The distance between majority class neighbors to anchor minority instances is used to identify nearest majority instances. These instances are used to compute the majority density factor, which is a critical factor in determining the importance of the neighbor. Overall, the algorithm applies a distance and density based weighting scheme. The weights calculated are a function of the relative distance between the nearest majority instance to anchor minority instance and its neighbors. This function also used the majority density factor. Most importantly, the density of the majority instances is raised to a power to control by a parameter α . The parameter α has seen greater flexibility in controlling the impact of density. It makes sure that the effect of density is not linearly penalized, making algorithm to capture more complex relationships in the majority class.

The minority neighbors are selected probabilistically using the cumulative weights. These weights are derived from the relative distance and density based approach. The probabilistic selection of minority neighbors increases the diversity of all minority instances in terms of getting selected. Proxima and Orion are selected based on these weights. This careful selection process helps the algorithm generate synthetic samples that maintain the complex characteristics of the minority class while considering the critical boundary regions.

In a subsequent phase, the Proxima and Orion instances are used to generate synthetic instances. A q-Gaussian weighting

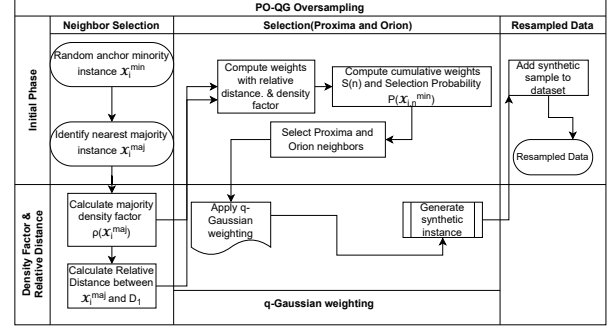


Fig. 2: Flow of PO-QG Algorithm: Synthetic Sample Generation

method applies the q-Gaussian distribution to the distances between the anchor instance and selected distant neighbors, Proxima and Orion. These q-Gaussian weights determine how the synthetic instances are formed by introducing a factor of non-linearity. These weights are then normalized for a well-balanced interpolation between the anchor and selected neighbors. This normalization ensures that the generated synthetic sample reflects the correct combination of the original data points. The q-Gaussian function ensures a smooth balance between the original and synthetic data by introducing flexibility in generating new instances.

This process is repeated iteratively to generate the desired number of synthetic instances. The algorithm combines these newly generated samples with the original dataset. The resampled dataset has equal instances of majority and minority classes without interrupting the minority class structure.

A. Weights Based on Distance and Density

Given an imbalanced dataset $D = \{(x_i, y_i)\}_{i=1}^N$, where $x_i \in \mathbb{R}^d$ is a d -dimensional feature vector and $y_i \in \{0, 1\}$ is the class label, the objective is to generate synthetic instances for the minority class to balance the class distribution. Let N_0 and N_1 denote the number of majority and minority class instances, respectively. To balance the dataset, the algorithm generates $\Delta N = N_0 - N_1$ synthetic minority class instances.

For each minority class instance x_i^{\min} (referred to as the anchor instance), the algorithm first identifies its k -nearest neighbors among other minority class instances:

$$N_k(x_i^{\min}) = \{x_{i_1}^{\min}, x_{i_2}^{\min}, \dots, x_{i_k}^{\min}\}, \quad (1)$$

Next, the nearest majority class instance x_i^{maj} to the anchor minority instance x_i^{\min} is identified as follows:

$$x_i^{\text{maj}} = \arg \min_{x_j \in D_0} |x_i^{\min} - x_j|, \quad (2)$$

where $D_0 = \{x_j \mid y_j = 0\}$ is the set of majority class instances. The density factor at each nearest majority instance x_i^{maj} is estimated using the distances to all other majority instances.:

$$\rho(x_i^{\text{maj}}) = \frac{1}{|D|} \sum_{x_j \in D_0} |x_i^{\text{maj}} - x_j|, \quad (3)$$

where x_i^{maj} is the nearest majority instance to anchor minority instance. This $\rho(x_i^{\text{maj}})$ value plays a key role in calculating the weights used in the neighbor selection process.

To compute the weight for each minority neighbor $x_{i,n}^{\text{min}} \in N_k(x_i^{\text{min}})$, the algorithm incorporates both the relative distance between the anchor minority instance and the majority instance, as well as the density of the majority class. The weight for each neighbor is calculated as:

$$w_{i,n} = \frac{|x_{i,n}^{\text{min}} - x_i^{\text{maj}}|}{|x_i^{\text{min}} - x_i^{\text{maj}}|} \cdot \frac{1}{\rho(x_i^{\text{maj}})^\alpha}, \quad (4)$$

Here, α is a parameter that controls the influence of the majority class density on the weighting. The first term in the equation 4 represents the relative distance between the minority neighbor $x_{i,n}^{\text{min}}$ and the nearest majority instance x_i^{maj} . This ratio serves as a measure of how important a minority instance is in relation to the anchor and its nearest majority neighbor. Using the relative distance, the algorithm can differentiate between boundary instances (relative distance close to 1) and outliers (relative distance much greater than 1). The second term adjusts this weight based on the density of the majority class, with higher densities lowering the weight. This ensures that synthetic samples are generated effectively near boundary regions where the classifier may struggle, while avoiding the influence of outliers or sparse regions in the minority class. The combined effect of relative distance and density penalization leads to a more balanced synthetic data generation.

Finally, the weights are normalized to ensure the sum to be 1:

$$\tilde{w}_{i,n} = \frac{w_{i,n}}{\sum_{m=1}^k w_{i,m}}, \quad (5)$$

This normalization also ensures that the weight distribution across all neighbors is balanced. The normalized weight $\tilde{w}_{i,n}$ reflects both the relative proximity of the minority neighbor to the majority instance and the density factor of the majority class, combining distance-based and density-based insights into the weighting scheme.

By carefully weighting the neighbors using this formulation, the algorithm ensures that the selection of two minority neighbors (Proxima and Orion) for generating synthetic instances that accounts for the structural relationship between minority and majority instances as well as the distributional characteristics of the minority class. This leads to the generation of synthetic samples that better reflect complex relationship between classes. This methodology improves the performance of classifiers trained on the resampled data.

B. Probability-Based Selection of Proxima and Orion

This section discusses the methodology for using cumulative weights to select two neighbors. This method introduces an element of randomness into the selection process, which helps

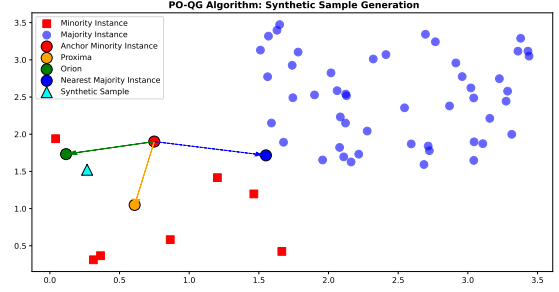


Fig. 3: Illustration of the PO-QG Algorithm: Synthetic Sample Generation

avoid bias towards only the nearest neighbors. Using both the distance and the density factor, cumulative weights enable the selection of neighbors that are closer and located in less dense areas of the majority class. This randomization helps overcome overfitting by introducing variability, preventing the algorithm from always selecting instances that could lead to overly similar synthetic instances.

a) *Cumulative Weight Calculation:* In order to encourage the selection process, cumulative weight function $S(n)$ for the n -th neighbor is defined as:

$$S(n) = \sum_{m=1}^n \tilde{w}_{i,m}, \quad (6)$$

where $\tilde{w}_{i,m}$ denotes the normalized weight of the m -th neighbor. This cumulative weight function $S(n)$ accumulates the normalized weights up to the n -th neighbor. The cumulative weights introduce randomness into the selection process, ensuring that neighbors with higher weights are more likely to be selected, while also allowing for a more diverse set of neighbors, even those not immediately adjacent to the minority instances.

b) *Selection Probability:* The probability of selecting the n -th neighbor $x_{i,n}^{\text{min}}$ is given by the difference in cumulative weights:

$$P(x_{i,n}^{\text{min}}) = S(n) - S(n-1), \quad (7)$$

where $S(0) = 0$. This probability ensures that neighbors with higher weights are more likely to be selected. The randomization introduced by the cumulative weight function prevents overfitting by allowing the algorithm to select not only boundary neighbors but also those from more varied regions of the feature space.

c) *Two Neighbors Selection:* Using the selection probabilities $P(x_{i,n}^{\text{min}})$, two neighbors x_{i,j_1}^{min} (Proxima) and x_{i,j_2}^{min} (Orion) are selected for synthetic sample generation. The process involves sampling based on the computed probabilities to choose the most representative Proxima and Orion instances.

Table I illustrates the cumulative weights and selection probabilities for the first three neighbors. The selection probabilities determines the two neighbors, x_{i,j_1}^{min} (Proxima) and

TABLE I: Example of Cumulative Weight Calculation and Selection Probability

Index n	Normalized Weight $\tilde{w}_{i,n}$	Cumulative Weight $S(n)$	Selection Probability $P(x_{i,n}^{\min})$
1	$\tilde{w}_{i,1}$	$\tilde{w}_{i,1}$	$\tilde{w}_{i,1}$
2	$\tilde{w}_{i,2}$	$\tilde{w}_{i,1} + \tilde{w}_{i,2}$	$\tilde{w}_{i,2}$
3	$\tilde{w}_{i,3}$	$\tilde{w}_{i,1} + \tilde{w}_{i,2} + \tilde{w}_{i,3}$	$\tilde{w}_{i,3}$

$x_{i,j2}^{\min}$ (Orion), chosen for generating synthetic samples based on their relative importance.

Figure 3 illustrates the steps involved in the PO-QG algorithm. The diagram shows how an anchor minority instance (red circle) selects its nearest neighbors, Proxima (orange circle) and Orion (green circle), based on the calculated selection probabilities. These neighbors are then used to generate a synthetic sample (blue triangle) that lies closer to the nearest minority instance in the feature space. This ensures that the synthetic sample is not only a relevant interpolation between minority instances but also strategically positioned in the sparse critical boundary regions to address the class imbalance.

Algorithm 1 displays the pseudocode for the selection of Proxima and Orion.

Algorithm 1 Selection of Proxima and Orion

- 1: **Input:** Minority dataset \mathcal{D}_1 , Majority dataset \mathcal{D}_0 , k , α
 - 2: **Output:** Two neighbors $x_{i,j1}^{\min}$ (Proxima) and $x_{i,j2}^{\min}$ (Orion)
 - 3: For each minority instance x_i^{\min} , identify its k -nearest neighbors $\mathcal{N}_k(x_i^{\min})$ using Eq. (1).
 - 4: Find the nearest majority instance x_i^{maj} according to Eq. (2).
 - 5: Estimate the density $\rho(x_i^{\text{maj}})$ using Eq. (3).
 - 6: Compute relative distance weights $w_{i,n}$ for each neighbor in $\mathcal{N}_k(x_i^{\min})$ using Eq. (4).
 - 7: Normalize the weights $\tilde{w}_{i,n}$ using Eq. (5).
 - 8: Compute cumulative weight $S(n)$ using Eq. (6).
 - 9: Select two neighbors $x_{i,j1}^{\min}$ (Proxima) and $x_{i,j2}^{\min}$ (Orion) based on selection probability according to Eq. (7).
-

C. q -Gaussian Distribution

We use the principles of the q -Gaussian distribution by utilizing its core q -exponential [33] structure to handle the distance between minority-class neighbors. This method enables the allocation of variable weights to instances based on their proximity and local distribution within given feature space. Our methodology addresses interpolation in sparse areas of the minority class by utilizing the characteristics of the heavy-tailed behavior of q -Gaussian distributions. This property helps adjust the overfitting risk to closely clustered minority instances. This is effective for distant instances, but they are still relevant and impact synthetic sample generation, unlike traditional Gaussian distributions that usually assume linear decay of impact with increasing distance. Our approach addresses nonlinearity by adjusting the intensity of influence as distance increases. This enables the algorithm to handle the complex patterns of various datasets more effectively.

a) *q -Gaussian Weights Calculation:* The q -Gaussian weights for the selected neighbors $x_{i,j1}^{\min}$ and $x_{i,j2}^{\min}$ are calculated as follows:

$$q(x_{i,j}) = \begin{cases} \exp\left(-\frac{1}{2}\left(\frac{\|x_{i,j}-x_i^{\min}\|}{\beta}\right)^2\right), & \text{if } q = 1 \\ \left[1 - (1-q)\left(\frac{\|x_{i,j}-x_i^{\min}\|}{\beta}\right)^2\right]^{\frac{1}{1-q}}, & \text{if } q \neq 1 \end{cases} \quad (8)$$

b) *q -Gaussian Weight Normalization:* The q -Gaussian weights are normalized as:

$$\tilde{q}_{i,j} = \frac{q(x_{i,j})}{q(x_{i,j1}^{\min}) + q(x_{i,j2}^{\min})}, \quad (9)$$

c) *Synthetic Sample Generation:* We generate a synthetic sample x_{syn} as a weighted combination of the selected neighbors $x_{i,j1}^{\min}$ and $x_{i,j2}^{\min}$:

$$x_{\text{syn}} = x_i^{\min} + \tilde{q}_{i,j1} \cdot (x_{i,j1}^{\min} - x_i^{\min}) + \tilde{q}_{i,j2} \cdot (x_{i,j2}^{\min} - x_i^{\min}). \quad (10)$$

d) *Repetition Process:* Repeat the Q -Gaussian weight calculation, normalization, and synthetic sample generation until the desired number of synthetic instances ΔN is generated.

D. Pseudocode of Algorithm

Algorithm 2 shows the pseudocode of PO-QG algorithm.

Algorithm 2 Proxima-Orion Q -Gaussian Oversampling (PO-QG)

- 1: **Input:**
 - Dataset (X, y)
 - Hyperparameters: k (number of neighbors), α (density scaling), β (smoothing for the q -Gaussian function), q (shapes the distribution)
 - 2: **Output:** Resampled dataset (X', y')
 - 3: **Initialize:**
 - $X_{\text{syn}} = \emptyset$ (Synthetic samples)
 - $y_{\text{syn}} = \emptyset$ (Synthetic labels)
 - 4: Extract minority instances D_1 and majority instances D_0
 - 5: **Nearest Neighbors Calculation:**
 - For each minority instance x_i in D_1
 - Find k nearest neighbors $\mathcal{N}_k(x_i)$ within D_1 using Eq. (1)
 - Identify nearest majority instances x_i^{maj} using Eq. (2)
 - Compute majority density factor $\rho(x_i^{\text{maj}})$ using Eq. (3)
 - 6: **Synthetic Sample Generation:**
 - While $|X_{\text{syn}}| < \Delta N$:
 - Refer algorithm 1 upto selection of Proxima and Orion
 - Apply q -Gaussian weighting (Eqs. 6–9) to calculate synthetic instances
 - Generate synthetic instance x_{syn} as a combination of anchor and Proxima-Orion
 - Add x_{syn} to X_{syn} , assign minority class label to y_{syn}
 - 7: **Return:** $X' \leftarrow X \cup X_{\text{syn}}$, $y' \leftarrow y \cup y_{\text{syn}}$
-

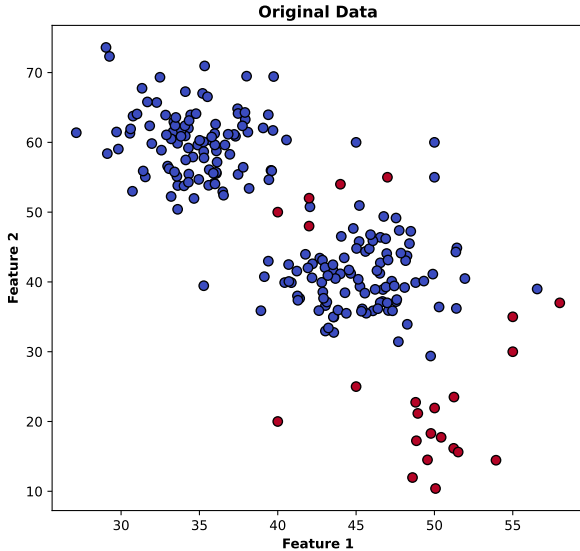


Fig. 4: Original Data

III. DATA ANALYSIS

To explain the key differences between PO-QG and some existing oversampling techniques, we present a case study utilizing an artificially imbalanced binary dataset. The generated dataset has 202 instances of the majority class and 23 instances of the minority class. In (Figure 4) red points represent the minority class instances, while blue points represent the majority class. The results of 6 different oversampling methods: PO-QG, SMOTE, SMOTE-TL, ADASYN, SMOTE-ENN, and Boundary SMOTE are shown in Figure 5.

This comparison provides several significant observations. The synthetic samples produced by PO-QG closely align with the original data distribution. This mainly helps in enhancing the separation between the majority and minority classes. The q-Gaussian weighting method ensures that more instances are generated near the decision boundary while allocating some instances across safer regions. This leads to a more natural integration of synthetic instances into the existing data without introducing excessive overlap into the majority class space. Moreover, SMOTE produces synthetic instances without accounting for the data distribution, potentially leading to the creation of instances within the majority class region. These instances may be considered noisy or overlapping, complicating the classification. SMOTE-TL tries to address the issue by removing instances near the decision boundary. Instead, it does not prioritize generating instances specifically in complex or boundary regions, leading to a more uniform but sometimes less effective distribution. ADASYN adapts to the data by generating more instances in regions of higher difficulty. This approach can also generate instances within the majority class region, resulting in overlapping clusters. SMOTE-ENN and Boundary SMOTE both concentrate on the boundary regions. However, they sometimes lack the refined control provided by the proposed weighting. SMOTE-ENN

eliminates noisy regions while generating synthetic instances more uniformly across the dataset. Boundary SMOTE focuses on the boundary regions but can generate clusters that sometimes extend into the majority region, lacking the fine-tuned balance that the proposed algorithm achieves.

IV. EXPERIMENTAL STUDY

This section evaluates the performance of the proposed algorithm via a series of assessments. We outline the performance metrics used in our analysis in Section [A]. Subsequently, we describe 42 selected small imbalanced datasets, eight large datasets, and three datasets derived from real-world applications in Section [B]. We then describe the parameter configurations for the algorithms that are used for comparison with PO-QG in this work in Section [C]. The experimental findings are presented in Section [D]. To assess the significance of the findings, we perform hypothesis tests to compare the outcomes of several training algorithms in Section [E]. Subsequently, the variable configurations of our proposed algorithm are examined in Section [F]. Ultimately, we present the results of our methodology applied to real-world imbalanced issues in Section [G].

A. Performance Metrics

While evaluating the performance of classifiers, it is essential to include metrics that provide more comprehensive view than simple accuracy, as accuracy alone can be misleading when dealing with imbalanced data. We utilize the confusion matrix to extract significant performance metrics. One such metric is the True Positive Rate (TPR), also known as recall, which discusses the ratio of accurately identified positive events [34], [35]. It is given by:

$$\text{TPR} = \frac{TP}{TP + FN} \quad (11)$$

We also consider the False Positive Rate (FPR), which refers to the ratio of inaccurately identified negative events and is calculated as:

$$\text{FPR} = \frac{FP}{FP + TN} \quad (12)$$

Subsequently, the G-Mean, a metric that balances the accuracy of both minority and majority class predictions, is computed by combining TPR and FPR:

$$\text{G-Mean} = \sqrt{\text{TPR} \times \text{FPR}} \quad (13)$$

Finally, we use the Area Under the Curve (AUC) metric, which is obtained from the Receiver Operating Characteristic (ROC) curve and is defined as:

$$\text{AUC} = \frac{\text{TPR} + \text{FPR}}{2} \quad (14)$$

G-Mean and AUC provide insightful information regarding the relationship between accurately identifying positive and negative instances. These metrics make them significant for evaluating performance in the framework of imbalanced learning models.

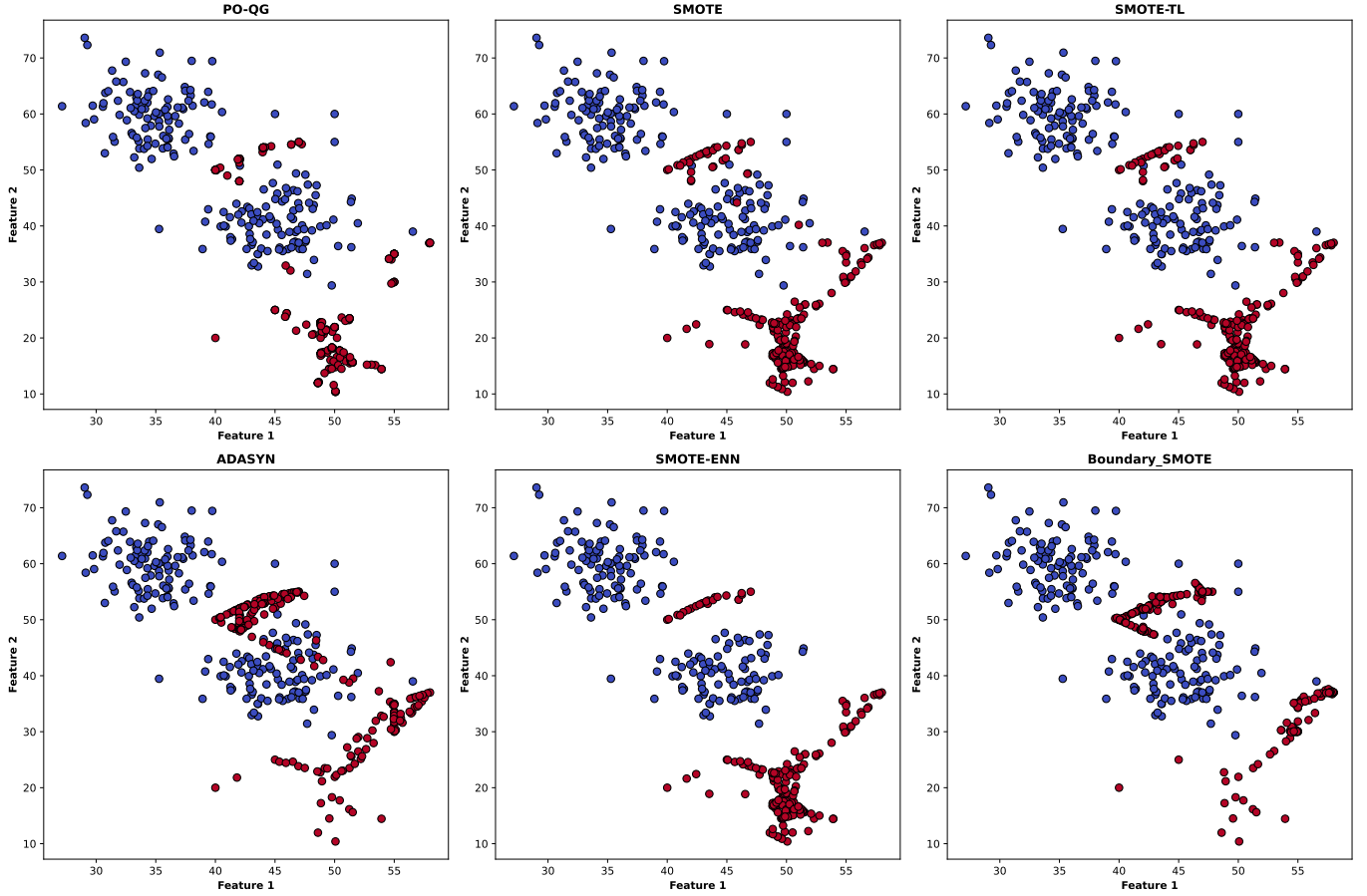


Fig. 5: Different Oversampling Methods: PO-QG, SMOTE, SMOTE-TL, ADASYN, SMOTE-ENN, and Boundary SMOTE.

B. Data sets

Performance of the proposed approach is assessed through the analysis of three distinct types of imbalanced datasets. The collection includes 42 small public datasets obtained from the KEEL data repository [36] and eight larger datasets sourced from the UCI Machine Learning Repository (<https://archive.ics.uci.edu/ml/index.php>). Furthermore, we include three datasets from real-world applications that were locally collected.

1) *Details of Small Datasets (KEEL)*: Table II presents comprehensive aspects of the 42 small datasets chosen from the KEEL repository, such as the number of data points (# datapoints), number of features (# features), and the Imbalance Ratio (I.R) [37] for each dataset. The I.R is the ratio of majority to minority class instances. It is widely used to measure the level of imbalance within datasets and is defined as:

$$I.R = \frac{n_{\text{maj}}}{n_{\text{min}}} \quad (15)$$

where n_{maj} and n_{min} denote the counts of instances belong to the majority and minority class instances, respectively. In the chosen datasets, 6 exhibit a low imbalance ($I.R \leq 2$), 13 display moderate imbalance ($I.R$ between 2 and 9), and 23 are characterized by high imbalance ($I.R > 9$). To ensure thorough evaluation, we implement five-fold cross-validation across all

datasets, with each model being trained on the training set and evaluated on the test set for each fold. The performance results are compiled to calculate AUC and G-Mean.

2) *UCI Large Datasets*: Alongside the small datasets, we use eight large datasets from the UCI Machine Learning Repository to evaluate our approach's effectiveness further. Each dataset comprises over 4,500 instances, two being high-dimensional and containing more than 50 features. Certain data sets are multi-class. In these scenarios, the remainder of classes are merged into the majority class, whereas the minority class is described as the one with the smallest number of instances. Detailed information regarding these large datasets is provided in Table III.

3) *Real Application Dataset*: The dataset used for this analysis were collected for a study in Jodhpur during 2015 and 2019 as part of Culturally Appropriate Geriatric Screening research [38]. The dataset included 111 older individuals living in the community, with 26% of the participants reporting falls in the last six months and 39% in the last two years. Eligibility criteria specified that participants must be 60 years of age or older. The dataset included essential subject characteristics such as age, gender, height, and weight, which were used to calculate Body Mass Index (BMI). Furthermore, participants completed a hand-timed 5STS (Sit to Stand) combined with three performance measures specified in the

TABLE II: Small Datasets(KEEL)

Dataset	# Datapoints	# Features	IR
abalone19	4174	8	129.44
abalone9-18	731	8	16.4
ecoli3	336	7	8.6
dermatology-6	358	34	16.9
ecoli-0_vs_1	220	7	1.86
ecoli1	336	7	3.36
ecoli4	336	7	15.8
flare-F	1066	11	23.79
glass-0-1-2-3_vs_4-5-6	214	9	3.2
glass-0-1-6_vs_2	192	9	10.29
glass-0-1-6_vs_5	184	9	19.44
glass0	214	9	2.06
glass1	214	9	1.82
glass2	214	9	11.59
glass4	214	9	15.47
glass5	214	9	22.78
glass6	214	9	6.38
haberman	306	3	2.78
new-thyroid1	215	5	5.14
newthyroid2	215	5	5.14
pima	768	8	1.87
segment0	2308	19	6.02
shuttle-c0-vs-c4	1829	9	13.87
vehicle0	846	18	3.25
vehicle1	846	18	2.9
vehicle2	846	18	2.88
vehicle3	846	18	2.99
vowel0	988	13	9.98
car-good	1728	6	24.04
winequality-red-4	1599	11	29.17
wisconsin	683	9	1.86
yeast-0-5-6-7-9_vs_4	528	8	9.35
yeast-1-2-8-9_vs_7	947	8	30.57
yeast-1-4-5-8_vs_7	693	8	22.1
yeast-1_vs_7	459	7	14.3
yeast-2_vs_4	514	8	9.08
yeast-2_vs_8	1484	8	28.1
yeast1	1484	8	2.46
yeast3	1484	8	8.1
yeast4	1484	8	28.1
yeast5	1484	8	32.73
yeast6	1484	8	41.4

TABLE III: Details of UCI Large Datasets

Dataset	# Datapoints	# Features	IR
statlog	6435	36	9.27
Waveform Database Generator (Version 1)	5000	21	2.035
Page Blocks Classification	5473	10	194.46
HTRU2	17898	8	9.92
Musk (Version 2)	6598	166	5.48
Letter Recognition	20000	16	26.24
Spambase	4601	57	1.53
Online Shoppers Purchasing Intention Dataset	12330	17	5.462

World Sarcopenia guidelines, which include gait speed, the SPPB (Short Physical Performance Battery) test, and the TUG (Time Up and Go) test, as mention in detail in Table IV.

Individuals were invited to participate in physical function assessments, conducted in a randomized order and interspersed with segments of a questionnaire focusing on previous medical history, general health condition, fear of falling, and history of falls. The history of falls was recorded through a questionnaire [39], which included 17 questions about the frequency of falls over the past six months to

one year. Additionally, the analysis included the historical background of each fall, describing the how, when, and where of each incident.

The gait velocity assessment requires individuals to walk a distance of 15 feet (4.57 meters) at their usual speed, ensuring they do not push themselves. Every participant undertook the test twice, and the highest score achieved was employed for all the analyses. For more details, see([38]).

TABLE IV: Real Application Datasets

Dataset	# Datapoints	# Features	IR
Gait Velocity	111	2	3.82
SPPB(Short Physical Performance Battery)	111	2	3.44
TUG(Time Up and Go)	111	2	21.2

C. Comparison Algorithms for the Experiment

We compared the proposed algorithm with five established oversampling algorithms. The algorithms and their corresponding parameter configurations are explained in Table V. The implementation of all oversampling algorithms uses the *Imbalanced-Learn (imblearn)* library [40], with *Support Vector Machine (SVM)* [41] acting as the primary learning model in these experiments. The SVM model utilizes the default radial basis function (RBF) kernel, configuring hyperparameters to their default settings.

TABLE V: Parameter Configuration of Traditional Algorithms

Algorithm	Parameters
SMOTE	k_neighbors = 5 (default), sampling_strategy = 'auto'
SMOTE-TL (SMOTETomek)	sampling_strategy = 'auto' (default)
ADASYN	n_neighbors = 5 (default), sampling_strategy = 'auto'
SMOTE-ENN	k_neighbors = 5 (default), sampling_strategy = 'auto'
Borderline SMOTE	kind = 'borderline-2' (default)

Each algorithm updates the training dataset by generating synthetic samples for the minority class through different methodologies. For example, SMOTE generates synthetic samples by interpolating existing minority samples, whereas SMOTE-Tomek combines SMOTE and Tomek links to enhance understanding of class boundaries. ADASYN shows the generation of additional synthetic samples in areas where the minority class is less densely populated. Borderline-SMOTE generates samples close to the decision boundary, especially in challenging classification regions. The evaluation of each algorithm's performance is carried out through the use of *Area Under the ROC Curve (AUC)* and *G-Mean*. The results are further elaborated in the following sections.

D. Performance Evaluation Using AUC and G-Mean Metrics

The AUC results for the 42 small datasets and the G-Mean results from the experimental study provide useful insights into the performance of different algorithms. One metric used to assess this performance is the count of datasets for which an algorithm attains the highest AUC, as illustrated in Table VI, and G-Mean, as presented in Table VII, referred to as its "winning times." These metrics suggest a noticeable comparison of the relative performance of each algorithm.

TABLE VI: AUC Performance Analysis for KEEL Data Sets

Algorithm	ADASYN	Boundary_SMOTE	SMOTE	SMOTE-ENN	SMOTE-TL	PO-QG
abalone19	0.8236446152	0.7406623171	0.8225460108	0.8169807984	0.8238861611	0.9174057688
abalone9-18	0.9000639127	0.8983010978	0.9037225102	0.8941176816	0.8957365093	0.942332681
ecoli3	0.9518032787	0.9491803279	0.9529976581	0.9558235753	0.9539266198	0.9743950039
dermatology-6	0.9992647059	0.9970258999	0.9985294118	0.9933384548	0.9992647059	0.9999882698
ecoli-0_vs_1	0.9885057471	0.9972413793	0.9967816092	0.9949425287	0.9963218391	0.9981609195
ecoli1	0.9441393288	0.946163273	0.9469032805	0.9460812594	0.9467816742	0.9665035822
ecoli4	0.9834945437	0.9897197421	0.9889880952	0.9850446429	0.9905381944	0.9976438492
flare-F	0.8746257771	0.8666234922	0.8754324087	0.8807663797	0.8725714703	0.9436395398
glass-0-1-2-3_vs_4-5-6	0.5898863636	0.4119318182	0.9699621212	0.966657197	0.9707007576	0.9695075758
glass-0-1-6_vs_2	0.4323809524	0.48	0.4457142857	0.5061904762	0.4352380952	0.5
glass-0-1-6_vs_5	0.7028571429	0.8342857143	0.6957142857	0.8771428571	0.62	0.9057142857
glass0	0.4	0.3522871217	0.3202498241	0.7143912738	0.2683497537	0.5
glass1	0.503117284	0.5033289242	0.4104585538	0.3855335097	0.4930952381	0.3755952381
glass2	0.3779487179	0.3062179487	0.3735042735	0.5875213675	0.396474359	0.4949358974
glass4	0.8699593496	0.8958536585	0.8682317073	0.8690650407	0.8640650407	0.902398374
glass5	0.856097561	0.7463414634	0.8426829268	0.656097561	0.756097561	0.893902439
glass6	0.9636036036	0.9018018018	0.9648648649	0.963963964	0.9630630631	0.9684684685
haberman	0.650629085	0.6469199346	0.6637009804	0.6689460784	0.6807107843	0.7208251634
new-thyroid1	0.9968253968	0.9976190476	0.9753968254	0.9587301587	0.9666666667	0.9904761905
newthyroid2	0.9841269841	0.9603174603	0.9555555556	0.946031746	0.953968254	0.9928571429
pima	0.8150006988	0.8116928721	0.8131893781	0.7967812718	0.8115104822	0.8305408805
segment0	0.9958719814	0.9869783864	0.9981833501	0.9982524755	0.9981986353	0.9984834954
shuttle-c0-vs-c4	0.9996345029	0.9991824613	0.9999882698	0.9999882698	0.9999882698	0.9999882698
vehicle0	0.9356115545	0.9305942847	0.9561732489	0.9421958396	0.9556240998	0.9678845695
vehicle1	0.7422903319	0.7413717843	0.7326487399	0.7298096245	0.7336039062	0.7489039162
vehicle2	0.8597795966	0.8341711433	0.8897628243	0.8691442733	0.8888896272	0.907261586
vehicle3	0.7369145717	0.7339210506	0.7407521734	0.7243048107	0.7363110134	0.7493109873
vowel0	0.9991358025	0.9995672115	0.9991347679	0.9990723498	0.9991964963	0.9997527416
car-good	0.9961820757	0.9968869635	0.9960200185	0.9953669197	0.9960596078	0.9986786971
winequality-red-4	0.6182209284	0.6503233019	0.6213671573	0.6090414828	0.6224923554	0.7221717393
wisconsin	0.9833585979	0.9816274522	0.987914885	0.9860959471	0.9859361643	0.9885995987
yeast-0-5-6-7-9_vs_4	0.8723877592	0.8674599282	0.8805221292	0.8706313796	0.8802460128	0.9237021531
yeast-1-2-8-9_vs_7	0.7632850242	0.7753306407	0.7704591352	0.7604755682	0.7724538687	0.8561089332
yeast-1-4-5-8_vs_7	0.7075814536	0.6823042455	0.7018740032	0.6762968026	0.6961209843	0.804427736
yeast-1_vs_7	0.8103511172	0.7994300046	0.8049475604	0.8192749658	0.8111354309	0.8949065207
yeast-2_vs_4	0.9826210209	0.9657826512	0.9785349994	0.978285095	0.9825338943	0.9908164393
yeast-2_vs_8	0.7204827022	0.7304114072	0.8246376812	0.8306393174	0.8290497896	0.9180282842
yeast1	0.7920995714	0.7911951427	0.7944617838	0.7955739395	0.7943340616	0.8174719433
yeast3	0.9734744665	0.9697255954	0.974420356	0.9727781324	0.9753473305	0.9810615319
yeast4	0.7632850242	0.7753306407	0.7704591352	0.7604755682	0.7724538687	0.8561089332
yeast5	0.986410108	0.9858314043	0.9866030093	0.9858699846	0.9857060185	0.9915219907
yeast6	0.9378723985	0.9330894711	0.9394651167	0.9393672763	0.9424238499	0.9727973137

Based on our analysis, three main observations become apparent. Initially, the proposed PO-QG method performs better than other algorithms, as fig 6 visually shows, attaining more "winning times" for AUC and G-Mean. PO-QG shows superior performance on most of datasets out of all the datasets as shown in Tables VI and VII. This shows its broad applicability and outstanding efficiency across various datasets. Furthermore, PO-QG shows a significant advantage over compared standard methods when applied to particular datasets, including *Abalone*, *winequality-red-4*, *flareF*, *glass-0-1-6 vs. 5*, *glass5*, *yeast-1-2-8-9 vs 7*, and *yeast-1-4-5-8 vs 7*. Secondly, PO-QG shows superior performance in dataset with significantly high imbalance ratios, attaining the highest AUC in 20 out of 23 datasets and achieving the highest G-Mean in 22 out of 23 datasets. The results highlight the efficient use of PO-QG in addressing the issues associated with highly imbalanced data, proving an advantage over all other methods

assessed in this scenario.

Lastly, PO-QG shows remarkable performance on different large instances datasets. It secures the highest AUC on all 8 datasets and G-Mean on 7 out of 8 large datasets, as illustrated in the Tables VIII and IX. The results on datasets such as *statlog* and *Waveform Database Generator (Version 1)* are interesting, showcasing significant advantages over other compared algorithms. PO-QG shows strong and consistent performance across imbalanced and large datasets.

E. Findings from Statistical Testing

The Wilcoxon signed-rank test (WS-RT), a non parametric test, is used to evaluate the statistical significance of the differences observed between PO-QG and the other methods [42], [43]. The evaluation involves determining if a critical difference exists between two sets of paired outcomes by computing the differences, ranking these differences, and

TABLE VII: GMean Performance Analysis for KEEL Data Sets

Algorithm	ADASYN	Boundary_SMOTE	SMOTE	SMOTE-ENN	SMOTE-TL	PO-QG
abalone19	0.6853842202	0.4705895633	0.6856925499	0.691974074	0.6864331238	0.8563934859
abalone9-18	0.8195828824	0.7724042715	0.8175250699	0.8060906255	0.8167095333	0.8447693753
ecoli3	0.9013671178	0.8894039799	0.8800860761	0.9032330608	0.8800726265	0.9365445303
dermatology-6	0.9704286486	0.8629587463	0.96294829	0.9614270911	0.9644578317	0.989545458
ecoli-0_vs_1	0.9723898138	0.982958187	0.9864367132	0.9864367132	0.9830761376	0.9864367132
ecoli1	0.8826759656	0.897300054	0.8910231035	0.881840625	0.8890791945	0.9176672388
ecoli4	0.8815750874	0.9077460888	0.8843581728	0.9051698002	0.8859518237	0.9670811805
flare-F	0.7532799824	0.7516803946	0.7549922529	0.7855809254	0.7559549437	0.8767567336
glass-0-1-2-3_vs_4-5-6	0.1524795068	0.8501805253	0.8394949811	0.1524795068	0.8394949811	0.8623977094
glass-0-1-6_vs_2	0.09561828875	0.4390800583	0.4457149103	0.1635798678	0.4390800583	0.4457149103
glass-0-1-6_vs_5	0	0.663923272	0.6670896317	0.1504786156	0.7217632693	0.8811809103
glass0	0.1114172029	0.5661275243	0.5802121034	0.1790749429	0.5741852624	0.6166767331
glass1	0.08451542547	0.3480945294	0.4561078239	0.1592234823	0.4267084014	0.4233115265
glass2	0.2022938932	0.5031591975	0.4932391147	0.1790749448	0.4932391147	0.4984361592
glass4	0.4939098913	0.8197788805	0.8708227448	0.1790749429	0.8708227448	0.8731230358
glass5	0.3135714703	0.5627276953	0.619877626	0	0.6159728052	0.8826382466
glass6	0.5471067931	0.6926776249	0.8837188606	0.09863939238	0.8811258864	0.8837584549
haberman	0.5573612838	0.5403001395	0.5290239532	0.6030977811	0.5584060895	0.5791659688
new-thyroid1	0.9572070979	0.9629683074	0.8694574927	0.8855906617	0.8979169398	0.9474777815
newthyroid2	0.9237611729	0.9238032183	0.8925898468	0.8833485479	0.866263202	0.9490333461
pima	0.7059459297	0.7146973758	0.718784333	0.7222956781	0.7133964051	0.7459627261
segment0	0.9458688783	0.9186197292	0.9855177644	0.9852754387	0.9850166074	0.9862883232
shuttle-c0-vs-c4	0.6770861487	0.3919183588	0.9991191568	0.9991191568	0.9988265451	0.9999882698
vehicle0	0.8014511726	0.7882436581	0.7907011119	0.7788320168	0.7926361846	0.8035159239
vehicle1	0.6656313166	0.6668219603	0.6616262852	0.6796443125	0.6635982139	0.6668945973
vehicle2	0.7818027028	0.7633600361	0.7585722738	0.7184330397	0.7584948743	0.7889238787
vehicle3	0.6671091839	0.6671533426	0.6667490312	0.6703390161	0.6640178396	0.6668428134
vowel0	0.9825833365	0.9774742727	0.980319875	0.9786125178	0.9791849245	0.9842873749
car-good	0.9739989545	0.9740114491	0.9735218381	0.9744162736	0.9744591841	0.9808853468
winequality-red-4	0.5920566952	0.5293836744	0.5524954833	0.5183284852	0.5735641562	0.6876298358
wisconsin	0.9739989545	0.9740114491	0.9735218381	0.9744162736	0.9744591841	0.9808853468
yeast-0-5-6-7-9_vs_4	0.7994191705	0.7777981898	0.7815399161	0.7990602312	0.7923019218	0.8305867899
yeast-1-2-8-9_vs_7	0.6781700901	0.6478257908	0.6724646927	0.682048722	0.6939549823	0.7598303082
yeast-1-4-5-8_vs_7	0.6576842758	0.5794626218	0.6445996748	0.6477476869	0.6425695132	0.7315357788
yeast-1_vs_7	0.7502948141	0.7026125362	0.7440621636	0.7467184966	0.7592448017	0.8198981413
yeast-2_vs_4	0.919892108	0.8527145237	0.8820938787	0.8814149594	0.8871626973	0.9392898792
yeast-2_vs_8	0.663700807	0.6448475147	0.7774467205	0.7457042783	0.7767002356	0.7805022446
yeast1	0.6967460885	0.692559266	0.7132166171	0.6958944014	0.7101086045	0.7229035217
yeast3	0.9249240373	0.9124404751	0.904980386	0.9212883967	0.917211754	0.9371226661
yeast4	0.6781700901	0.6478257908	0.6724646927	0.682048722	0.6939549823	0.7598303082
yeast5	0.9614817303	0.9586504492	0.9614650623	0.9732368721	0.9614862957	0.9785682226
yeast6	0.8580471542	0.8809659591	0.8613848872	0.8679942466	0.876289959	0.8696335967

TABLE VIII: AUC Performance Analysis for Large Data Sets

Algorithm	ADASYN	Boundary_SMOTE	SMOTE	SMOTE-ENN	SMOTE-TL	PO-QG
statlog	0.9439989376	0.9437396329	0.9488187454	0.9448510662	0.9480395379	0.9626004194
Waveform Database Generator (Version 1)	0.9705675935	0.9675808798	0.972206531	0.9677053986	0.9725354656	0.9826452375
Page Blocks Classification	0.9993449648	0.9981083563	0.9993082339	0.9991735537	0.9993082339	0.9998102234
HTRU2	0.9616153272	0.9679756726	0.9651454246	0.9635094904	0.9653548545	0.9708489868
Musk (Version 2)	0.9948499955	0.993580835	0.9948857203	0.9901492462	0.9942606724	0.99718392
Letter Recognition	0.9932491519	0.9886441273	0.9944131983	0.9940575587	0.9944069761	0.9981736233
Spambase	0.9770863574	0.9761556881	0.9745218345	0.9676248822	0.9747343672	0.9778603157
Online Shoppers Purchasing Intention Dataset	0.8841737462	0.8824871254	0.8820982419	0.8841797609	0.8834109209	0.8853129385

TABLE IX: GMean Performance Analysis for Large Data Sets

Algorithm	ADASYN	Boundary_SMOTE	SMOTE	SMOTE-ENN	SMOTE-TL	PO-QG
statlog	0.8784187588	0.8821120244	0.883282562	0.8779933443	0.884533952	0.9082936169
Waveform Database Generator (Version 1)	0.9089474172	0.9005209421	0.9100254444	0.9012295213	0.9112215805	0.9357023912
Page Blocks Classification	0.996780648	0.9208639896	0.9973332216	0.9971490163	0.9973333067	0.9978856676
HTRU2	0.9003554519	0.9304246492	0.9422261132	0.9420682432	0.9427270401	0.9442228958
Musk (Version 2)	0.9812825416	0.974242721	0.9749786075	0.9629164812	0.9749357079	0.9867915506
Letter Recognition	0.9598796446	0.9497138448	0.9615448309	0.9627244055	0.9620368819	0.9797969721
Spambase	0.9335865229	0.9259853723	0.9267307093	0.9115141265	0.92646572	0.93477728
Online Shoppers Purchasing Intention Dataset	0.8298853189	0.8282348681	0.8315539366	0.8357185055	0.8312241233	0.8334298959

TABLE X: PO-QG Versus Compared Methods: WS-RT Results

AUC				G-mean			
Comparison	R+	R-	p-value	Comparison	R+	R-	p-value
PO-QG vs ADASYN	2.2719	0.1339	2.02E-10	PO-QG vs ADASYN	6.1128	0.0109	2.43E-13
PO-QG vs Boundary_SMOTE	2.7003	0.1349	1.44E-10	PO-QG vs Boundary_SMOTE	3.8061	0.0319	6.62E-12
PO-QG vs SMOTE	1.8182	0.0353	8.69E-09	PO-QG vs SMOTE	2.0715	0.0337	1.59E-08
PO-QG vs SMOTE-ENN	1.6525	0.3231	9.15E-07	PO-QG vs SMOTE-ENN	7.4470	0.0425	1.47E-08
PO-QG vs SMOTE-TL	2.0173	0.1187	2.33E-08	PO-QG vs SMOTE-TL	1.8986	0.0110	4.91E-12

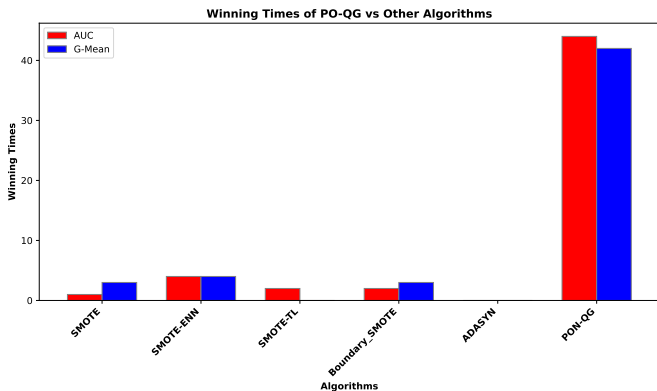


Fig. 6: Winning times of PO-QG vs Other Algorithms

separately summing the ranks for positive (R^+) and negative (R^-) differences. A significant difference between R^+ and R^- indicates that one approach consistently surpasses the performance of the other. The null hypothesis states no significant difference between the two methods. It is evaluated by comparing the p-value.

The results presented in Table X indicate that PO-QG consistently surpasses the other methods in terms of both AUC and G-Mean. The R^+ values for all comparisons in AUC are notably higher than the R^- values, and the p-values are very small indicating that the performance of PO-QG is significantly better. For instance, compared to ADASYN, the R^+ value stands at 2.27, whereas R^- is merely 0.13, with a p-value of $2.02E - 10$. Similarly, comparisons with Boundary_SMOTE, SMOTE and SMOTE-ENN yield p-values significantly low, confirming the superiority of PO-QG.

The pattern continues for G-Mean, with PO-QG showing significant improvements as compared to all baseline methods. The findings indicate that PO-QG accurately shows superior performance across all the datasets.

F. Parameter Configurations for the Proposed Algorithm

The parameters selected for the proposed algorithm— k , α , β , and q —were determined through a systematic optimization process utilizing grid search techniques. This process assessed various values for each parameter to identify the best configuration for each dataset in table XI. Grid search investigates various parameter ranges, including k (number of nearest neighbors), α (controlling density adjustment), β (smoothing for the q -Gaussian function), and q (shapes the distribution), enabling the algorithm to adapt itself to the specific features of each dataset.

TABLE XI: Parameter Configurations for the Proposed Algorithm

Dataset	k	α	β	q
abalone19	5	0.5	0.1	1.7
abalone9-18	5	0.7	0.2	1.3
ecoli3	5	0.3	0.05	1.3
dermatology-6	5	0.3	0.05	1.3
ecoli-0_vs_1	5	0.3	0.05	1.3
ecoli1	10	0.7	0.05	1.3
ecoli4	5	0.3	0.2	1.3
flare-F	5	0.5	0.05	1.3
glass-0-1-2-3_vs_4-5-6	10	0.5	0.2	1.5
glass-0-1-6_vs_2	5	0.3	0.05	1.3
glass-0-1-6_vs_5	5	0.7	0.2	1.3
glass0	5	0.3	0.05	1.3
glass1	5	0.7	0.2	1.3
glass2	5	0.7	0.1	1.7
glass4	5	0.3	0.1	1.7
glass5	10	0.7	0.1	1.7
glass6	5	0.3	0.05	1.3
haberman	5	0.3	0.2	1.7
new-thyroid1	5	0.5	0.1	1.3
newthyroid2	5	0.5	0.1	1.3
pima	10	0.5	0.1	1.7
segment0	5	0.3	0.1	1.3
shuttle-c0-vs-c4	5	0.3	0.05	1.3
vehicle0	5	0.3	0.05	1.5
vehicle1	5	0.3	0.05	1.5
vehicle2	5	0.3	0.1	1.5
vehicle3	5	0.3	0.1	1.5
vowel0	5	0.3	0.2	1.5
car-good	5	0.3	0.05	1.5
winequality-red-4	10	0.3	0.1	1.5
wisconsin	7	0.3	0.05	1.3
yeast-0-5-6-7-9_vs_4	5	0.3	0.1	1.5
yeast-1-2-8-9_vs_7	5	0.3	0.05	1.7
yeast-1-4-5-8_vs_7	7	0.3	0.05	1.5
yeast-1_vs_7	5	0.3	0.1	1.5
yeast-2_vs_4	5	0.3	0.1	1.7
yeast-2_vs_8	7	0.5	0.1	1.3
yeast1	5	0.3	0.05	1.3
yeast3	5	0.5	0.05	1.5
yeast4	5	0.5	0.05	1.7
yeast5	10	0.7	0.05	1.3
yeast6	7	0.7	0.1	1.7
Letter Recognition	5	0.3	0.1	1.7
spambase	5	0.5	0.2	1.7
Online Shoppers Purchasing Intention Dataset	5	0.5	0.2	1.7
HTRU2	7	0.3	0.2	1.7
statlog	5	0.7	0.1	1.3
Page Blocks Classification	10	0.3	0.1	1.3
Waveform Database Generator (Version 1)	5	0.3	0.05	1.3
Musk (Version 2)	5	0.3	0.1	1.5

From the analysis of the parameter configurations, several significant patterns are observed. In the majority of datasets, a value of k is typically established at 5, indicating that a limited neighborhood effectively captures local patterns. In

the case of more complex datasets like *ecoli1*, *glass-0-1-2-3_vs_4-5-6*, and *winequality-red-4*, a larger $k = 10$ is chosen, indicating that these datasets gain from a wider neighborhood for improved generalization. Intermediate values of k , like 7 in *wisconsin* and *yeast6*, highlight the importance for a balance between small and large neighborhoods to accurately represent the structure of these datasets. The parameter α , which controls density adjustment, generally falls within the range of 0.3 to 0.7. Typically, α is established at 0.3, indicating a moderate density adjustment appropriate for dataset that do not require significant weighting. In the case of datasets such as *abalone19*, *flare-F*, and *spambase*, a higher α value of 0.5 is chosen, reflecting the need for increased density influence as a result of the more complex or imbalanced nature of the data. In certain instances, like *ecoli1* and *glass1*, a higher α value of 0.7 is applied, indicating that these dataset require more accurate density adjustments, because of their more significant levels of imbalance or scattered data points. The β parameter, which affects the q -Gaussian smoothing, typically ranges from 0.05 to 0.2. The standard β values (0.05 or 0.1) suggest a gentle smoothing approach, resulting in only minor adjustments to the data distribution. This is adequate for datasets where significant modifications might hinder model performance. In specific datasets, including *abalone9-18* and *glass-0-1-6_vs_5*, a higher β value of 0.2 is noted, suggesting the need for improved control over the distribution tails, probably to address outliers or skewed distributions. The q parameter, which defines the shape of the q -Gaussian distribution, typically falls within the range of 1.3 to 1.7. Many dataset tend to show values around 1.3 or 1.5, suggesting that these datasets display non-normal distributions. In datasets such as *abalone19*, *glass2*, and *haberman*, a higher q value of 1.7 indicates the likelihood of outliers or a heavier-tailed distribution, requiring the algorithm to adjust for more extreme data points.

In order to gain a clearer understanding of the behavior of each dataset with these parameters, we categorize the dataset into representatives (Fig 7) and high variance groups (Fig 8). In the selection of these datasets, a systematic approach is utilized, guided by statistical criteria. We compute the mean and standard deviation for each parameter (k , α , β , and q) across all representative dataset. Subsequently, we identified dataset with parameter values that were within one standard deviation of the mean, ensuring a balanced representation of the overall characteristics of the dataset. On the other hand, for datasets with high variance, we focus on those where the parameters varied by more than one standard deviation from the mean, indicating significant variability. In order to have an attainable analysis size, we randomly selected a smaller number of dataset from both groups, ensuring a diverse yet focused representation for subsequent analysis. This approach allows a thorough examination of the algorithm’s effectiveness across various dataset characteristics, reducing bias and improving clarity.

Consequently, the parameter configurations indicate the adaptability of the proposed algorithm to meet particular demands of each dataset. Lower values of k along with moderate α and β suggest that many dataset can be accurately

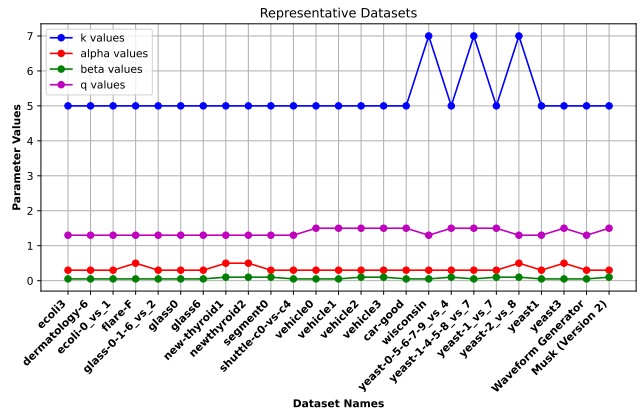


Fig. 7: Representative Datasets

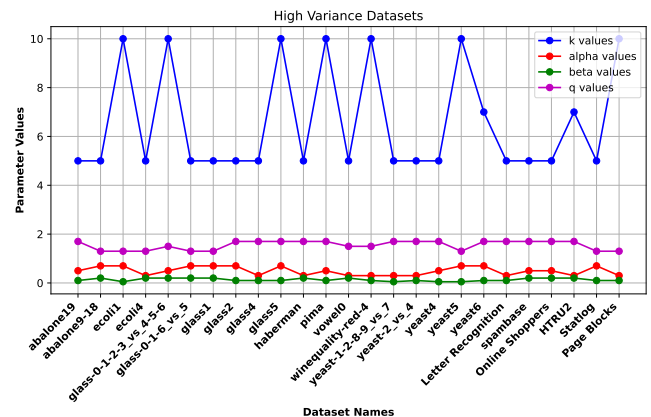


Fig. 8: High Variance Datasets

represented by focusing on local patterns and implementing slight density modifications. In the case of more intricate dataset, it is essential to utilize higher values of k , α , and q to effectively address components such as imbalance, outliers, or irregular distributions. By adjusting these parameters the algorithm ensures strong performance across diverse datasets, successfully tackling issues like data imbalance, complexity, and noise.

G. Results of Applications on Real-World Imbalanced Data

The practicality of proposed algorithm as assessed on real-world imbalanced datasets. We implement PO-QG on the dataset we gathered, explicitly focusing on assessing the risk of sarcopenia through gait speed, the Short Physical Performance Battery (SPPB) test, and the Time Up and Go (TUG) test. The visual representation of PO-QG’s performance is achieved through radar plots, as illustrated in Fig 9, 10 and 11 respectively. The proposed algorithm performs better, attaining the highest AUC and G-Mean values across all three datasets. The findings indicate PO-QG’s capacity to identify individuals at risk of sarcopenia accurately. PO-QG’s ability to surpass other algorithms shows its potential for improved sarcopenia

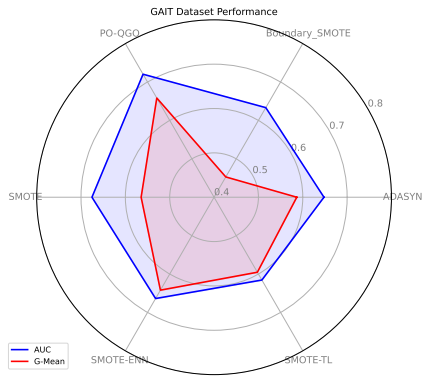


Fig. 9: Result Gait Dataset

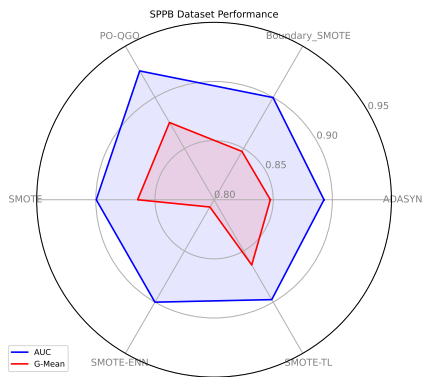


Fig. 10: Result SPPB Dataset

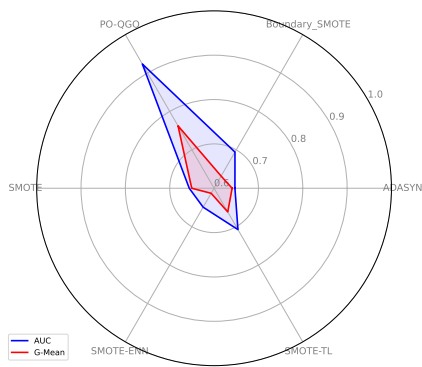


Fig. 11: Result TUG Dataset

risk detection, essential for timely intervention and improved patient outcomes.

V. CONCLUSION

A novel oversampling method, PO-QG, has been introduced to address the challenge of imbalanced data classification.

The essential characteristics of PO-QG originate in its unique neighbor selection and probabilistic nature. The process involves carefully selecting two instances, Proxima and Orion, and generating new samples according to probability and using q-Gaussian distribution, utilizing information from various minority instances. Furthermore, the synthetic data generation closely resembles the distribution of the original dataset, ensuring that the newly created samples align effectively with the actual data patterns.

We evaluated our method alongside five other approaches for handling imbalanced learning, utilizing 42 small and eight large imbalanced datasets for comparison. Experimental results consistently demonstrate that PO-QG shows improved outcomes regarding AUC and G-Mean. Furthermore, research investigations utilizing three real-world datasets for sarcopenia risk assessment—gait speed, the Short Physical Performance Battery (SPPB) test, and the Time Up and Go (TUG) test—demonstrate the effectiveness of PO-QG in recognizing fall risk. The accuracy improvement across most datasets indicates its significance.

However, the existing implementation of PO-QG might show some research gaps like a comparatively increased time complexity or execution duration when compared with other conventional algorithms and use of more advance and accurate optimization of parameters, something that we plan to address in future work efforts. We aim to create an improved PO-QG version that improves speed and efficiency while maintaining higher classification performance.

REFERENCES

- [1] S. Abokadr, A. Azman, H. Hamdan, and N. Amelina, "Handling Imbalanced Data for Improved Classification Performance: Methods and Challenges," in *2023 3rd International Conference on Emerging Smart Technologies and Applications (eSmarTA)*, pp. 1–8, Oct. 2023.
- [2] Y. J. Kim, "Machine Learning Models for Sarcopenia Identification Based on Radiomic Features of Muscles in Computed Tomography," *International Journal of Environmental Research and Public Health*, vol. 18, p. 8710, Jan. 2021.
- [3] S. Nami and M. Shajari, "Cost-sensitive payment card fraud detection based on dynamic random forest and k -nearest neighbors," *Expert Systems with Applications*, vol. 110, pp. 381–392, Nov. 2018.
- [4] F. Thabtah, S. Hammoud, F. Kamalov, and A. Gonsalves, "Data imbalance in classification: Experimental evaluation," *Information Sciences*, vol. 513, pp. 429–441, Mar. 2020.
- [5] B. Krawczyk, "Learning from imbalanced data: open challenges and future directions," *Progress in Artificial Intelligence*, vol. 5, pp. 221–232, Nov. 2016.
- [6] A. Kulkarni, D. Chong, and F. A. Batarseh, "5 - Foundations of data imbalance and solutions for a data democracy," in *Data Democracy* (F. A. Batarseh and R. Yang, eds.), pp. 83–106, Academic Press, Jan. 2020.
- [7] N. Thai-Nghe, Z. Gantner, and L. Schmidt-Thieme, "Cost-sensitive learning methods for imbalanced data," in *The 2010 International Joint Conference on Neural Networks (IJCNN)*, pp. 1–8, July 2010.
- [8] J. Tanha, Y. Abdi, N. Samadi, N. Razzaghi, and M. Asadpour, "Boosting methods for multi-class imbalanced data classification: an experimental review," *Journal of Big Data*, vol. 7, p. 70, Sept. 2020.
- [9] J. L. Leevy, T. M. Khoshgoftaar, R. A. Bauder, and N. Seliya, "A survey on addressing high-class imbalance in big data," *Journal of Big Data*, vol. 5, p. 42, Nov. 2018.
- [10] X.-Y. Liu, J. Wu, and Z.-H. Zhou, "Exploratory Undersampling for Class-Imbalance Learning," *IEEE Transactions on Systems, Man, and Cybernetics, Part B (Cybernetics)*, vol. 39, pp. 539–550, Apr. 2009.
- [11] M. T. Vo, T. Nguyen, H. A. Vo, and T. Le, "Noise-adaptive synthetic oversampling technique," *Applied Intelligence*, vol. 51, pp. 7827–7836, Nov. 2021.

- [12] N. V. Chawla, K. W. Bowyer, L. O. Hall, and W. P. Kegelmeyer, "SMOTE: Synthetic Minority Over-sampling Technique," *Journal of Artificial Intelligence Research*, vol. 16, pp. 321–357, June 2002.
- [13] Y. Sanganmak and A. Hanskunatai, "DBSM: The combination of DBSCAN and SMOTE for imbalanced data classification," in *2016 13th International Joint Conference on Computer Science and Software Engineering (JCSSE)*, pp. 1–5, July 2016.
- [14] Z. Xu, D. Shen, T. Nie, and Y. Kou, "A hybrid sampling algorithm combining M-SMOTE and ENN based on Random forest for medical imbalanced data," *Journal of Biomedical Informatics*, vol. 107, p. 103465, July 2020.
- [15] L. Tao, H. Zhu, Q. Wang, Y. Liang, and X. Deng, "A Combined Priori and Purity Gaussian OverSampling Algorithm for Imbalanced Data Classification," *IEEE Access*, vol. 11, pp. 130688–130696, 2023.
- [16] H. Majzoub and I. Elgedawy, "AB-SMOTE: An Affinitive Borderline SMOTE Approach for Imbalanced Data Binary Classification," *International Journal of Machine Learning and Computing*, vol. 10, pp. 31–37, Jan. 2020.
- [17] C. Rao, X. Wei, X. Xiao, Y. Shi, and M. Goh, "Oversampling method via adaptive double weights and Gaussian kernel function for the transformation of unbalanced data in risk assessment of cardiovascular disease," *Information Sciences*, vol. 665, p. 120410, Apr. 2024.
- [18] Y. Liu, Y. Liu, B. X. B. Yu, S. Zhong, and Z. Hu, "Noise-robust oversampling for imbalanced data classification," *Pattern Recognition*, vol. 133, p. 109008, Jan. 2023.
- [19] Y. Xie, M. Qiu, H. Zhang, L. Peng, and Z. Chen, "Gaussian Distribution Based Oversampling for Imbalanced Data Classification," *IEEE Transactions on Knowledge and Data Engineering*, vol. 34, pp. 667–679, Feb. 2022.
- [20] M. Koziarski, "CSMOUTE: Combined Synthetic Oversampling and Undersampling Technique for Imbalanced Data Classification," in *2021 International Joint Conference on Neural Networks (IJCNN)*, pp. 1–8, July 2021.
- [21] D. Devi, S. K. Biswas, and B. Purkayastha, "Correlation-based Oversampling aided Cost Sensitive Ensemble learning technique for Treatment of Class Imbalance," *Journal of Experimental & Theoretical Artificial Intelligence*, vol. 34, pp. 143–174, Jan. 2022.
- [22] A. Jurek, Y. Bi, S. Wu, and C. Nugent, "A survey of commonly used ensemble-based classification techniques," *The Knowledge Engineering Review*, vol. 29, pp. 551–581, Nov. 2014.
- [23] R. Nithya, T. Kokilavani, and T. L. A. Beena, "Balancing cerebrovascular disease data with integrated ensemble learning and SVM-SMOTE," *Network Modeling Analysis in Health Informatics and Bioinformatics*, vol. 13, p. 12, Mar. 2024.
- [24] X. Liang, Y. Gao, and S. Xu, "ASE: Anomaly Scoring Based Ensemble Learning for Imbalanced Datasets," Aug. 2022.
- [25] Y.-X. He, D.-X. Liu, S.-H. Lyu, C. Qian, and Z.-H. Zhou, "Multi-class imbalance problem: A multi-objective solution," *Information Sciences*, vol. 680, p. 121156, Oct. 2024.
- [26] N. H. A. Malek, W. F. W. Yaacob, Y. B. Wah, S. A. Md Nasir, N. Shaadan, and S. W. Indratno, "Comparison of ensemble hybrid sampling with bagging and boosting machine learning approach for imbalanced data," *Indonesian Journal of Electrical Engineering and Computer Science*, vol. 29, p. 598, Jan. 2022.
- [27] S. H. Khan, M. Hayat, M. Bennamoun, F. A. Sohel, and R. Togneri, "Cost-Sensitive Learning of Deep Feature Representations From Imbalanced Data," *IEEE Transactions on Neural Networks and Learning Systems*, vol. 29, pp. 3573–3587, Aug. 2018.
- [28] A. Fernández, S. García, M. Galar, R. C. Prati, B. Krawczyk, and F. Herrera, "Cost-Sensitive Learning," in *Learning from Imbalanced Data Sets* (A. Fernández, S. García, M. Galar, R. C. Prati, B. Krawczyk, and F. Herrera, eds.), pp. 63–78, Cham: Springer International Publishing, 2018.
- [29] Z. Hou, J. Tang, Y. Li, S. Fu, and Y. Tian, "MVQS: Robust multi-view instance-level cost-sensitive learning method for imbalanced data classification," *Information Sciences*, vol. 675, p. 120467, July 2024.
- [30] K. Yang, Z. Yu, W. Chen, Z. Liang, and C. L. P. Chen, "Solving the Imbalanced Problem by Metric Learning and Oversampling," *IEEE Transactions on Knowledge and Data Engineering*, pp. 1–14, 2024.
- [31] X. Li and Q. Liu, "DDSC-SMOTE: an imbalanced data oversampling algorithm based on data distribution and spectral clustering," *The Journal of Supercomputing*, vol. 80, pp. 17760–17789, Aug. 2024.
- [32] M. Steinbach and P.-N. Tan, "kNN: k-Nearest Neighbors," in *The Top Ten Algorithms in Data Mining*, Chapman and Hall/CRC, 2009.
- [33] W. P. Johnson, "Some applications of the q -exponential formula," *Discrete Mathematics*, vol. 157, pp. 207–225, Oct. 1996.
- [34] T. Hernández-Del-Toro, F. Martínez-Santiago, and A. Montejó-Ráez, "Chapter 7 - Assessing classifier's performance," in *Biosignal Processing and Classification Using Computational Learning and Intelligence* (A. A. Torres-García, C. A. Reyes-García, L. Villaseñor-Pineda, and O. Mendoza-Montoya, eds.), pp. 131–149, Academic Press, Jan. 2022.
- [35] G. Canbek, T. Taskaya Temizel, and S. Sagiroglu, "PToPI: A Comprehensive Review, Analysis, and Knowledge Representation of Binary Classification Performance Measures/Metrics," *SN Computer Science*, vol. 4, p. 13, Oct. 2022.
- [36] "KEEL: A software tool to assess evolutionary algorithms for Data Mining problems (regression, classification, clustering, pattern mining and so on)."
- [37] N. Noorhalim, A. Ali, and S. M. Shamsuddin, "Handling Imbalanced Ratio for Class Imbalance Problem Using SMOTE," in *Proceedings of the Third International Conference on Computing, Mathematics and Statistics (iCMS2017)* (L.-K. Kor, A.-R. Ahmad, Z. Idrus, and K. A. Mansor, eds.), (Singapore), pp. 19–30, Springer, 2019.
- [38] B. K. Shukla, H. Jain, V. Vijay, S. K. Yadav, A. Mathur, and D. J. Hewson, "A Comparison of Four Approaches to Evaluate the Sit-to-Stand Movement," *IEEE Transactions on Neural Systems and Rehabilitation Engineering*, vol. 28, pp. 1317–1324, June 2020.
- [39] A. H. Myers, S. P. Baker, M. L. Van Natta, H. Abbey, and E. G. Robinson, "Risk Factors Associated with Falls and Injuries among Elderly Institutionalized Persons," *American Journal of Epidemiology*, vol. 133, pp. 1179–1190, June 1991.
- [40] G. Lemaître, F. Nogueira, and C. K. Aridas, "Imbalanced-learn: A Python Toolbox to Tackle the Curse of Imbalanced Datasets in Machine Learning," *Journal of Machine Learning Research*, vol. 18, no. 17, pp. 1–5, 2017.
- [41] S. Yue, P. Li, and P. Hao, "SVM classification: Its contents and challenges," *Applied Mathematics-A Journal of Chinese Universities*, vol. 18, pp. 332–342, Sept. 2003.
- [42] D. J. Sheskin, *Handbook of Parametric and Nonparametric Statistical Procedures: Third Edition*. New York: Chapman and Hall/CRC, 3 ed., Aug. 2003.
- [43] L. Wasserman, *All of Nonparametric Statistics*. Springer Science & Business Media, Sept. 2006.